Available online at www.sciencedirect.com

ScienceDirect

Procedia Structural Integrity 28 (2020) 1559–1571

Structural Integrity Procedia

www.elsevier.com/locate/procedia

1st Virtual European Conference on Fracture

Peridynamic modelling of Hertzian indentation fracture

Wei Lu[a,b,*], Selda Oterkus[a], Erkan Oterkus[a]

[a]*PeriDynamics Research Centre, Department of Naval Architecture, Ocean and Marine Engineering, University of Strathclyde, 100 Montrose Street, Glasgow G4 0LZ, UK*

[b]*College of Shipbuilding Engieering, Harbin Engineering University, Harbin, China*

Abstract

Hertzian indentation technique is a method that is widely used in the investigation of the fracture toughness and the Young's modulus of a brittle material. Thus, it has been studied in various research studies during the past century. The problem describes axisymmetric fracture behaviour of a flaw-free brittle solid under compression due to the impact of a stiff indenter. During the fracture process, the evolution of the crack is divided into two stages. Initially, a ring crack forms spontaneously outside the contact region under a critical load. Then, it propagates for a small distance perpendicular to the free surface of the brittle solid. With the increase in load applied on the indenter, a cone-shaped crack occurs at the bottom of the ring flaw and it grows at a certain angle. Hence, in this study a new numerical technique, peridynamics, is utilised to analyse the historical complex fracture problem. To reduce the computational time, the problem is simplified by considering an axisymmetric model. The effect of Poisson's ratio on the orientation and size of the cone-shaped crack are investigated.

Keywords: Peridynamics; Hertzian; Indentation; Fracture

* Corresponding author. Tel.: +44-141-548-3876.
E-mail address: wei.lu@strath.ac.uk

10.1016/j.prostr.2020.10.128

1. Introduction

Hertzian indentation technique is a method that is widely used in the investigation of the fracture toughness and the Young's modulus of a brittle material (Warren, 1978, 1995; Oliver and Pharr, 1992). Thus, it has been studied in various research studies during the past century. The problem describes axisymmetric fracture behaviour of a flaw-free brittle solid under compression due to the impact of a stiff indenter. During the fracture process, the evolution of the crack is divided into two stages as shown in Fig. 1. Initially, a ring crack forms spontaneously outside the contact region under a critical load. Then, it propagates for a small distance perpendicular to the free surface of the brittle solid. With the increase in load applied on the indenter, a cone-shaped crack occurs at the bottom of the ring flaw and it grows at a certain angle. Both theoretical and numerical methods have been utilized to investigate the Hertzian indentation fracture. Fracture mechanics was applied by Frank and Lawn (1967) to analyse the Hertzian fracture. Kocer and Collins (1998) investigated the angle of cone-shaped crack with finite element method. They found that the cracks would propagate along the path with maximum release of strain energy. Boundary element technique coupled with criteria for initiation of crack extension and orientation of crack was implemented by Selvadurai (2000) to analyse the growth of the crack. A two-dimensional axisymmetric extended finite element model was proposed by Tumbajoy-Spinel et al. (2013) to model Hertzian cone crack propagation. Phase field method (Strobl and Seelig, 2019) was used to model the Hertzian fracture as well. In this study, peridynamics (Basoglu et. al., 2019; De Meo et. al., 2017; Diyaroglu et. al., 2017a,b, 2019; Imachi et. al., 2019; Oterkus et. al., 2010a,b, 2012, 2014; Oterkus and Madenci, 2012a,b; Vazic et. al., 2017; Wang et. al., 2018; Yang et. al., 2019; Zhu et. al., 2016) is utilized to simulate the Hertzian indentation fracture problem due to its advantage of dealing with problems with discontinuities. Since the equation of motion of peridynamics is in integral form, without spatial derivative terms, it is always valid. No additional crack growth law is needed to predict the damage. Thus, it is suitable to model fracture problems. In this paper, in order to reduce computation time, the two-dimensional axisymmetric peridynamic model is utilized to model the Hertzian indentation fracture.

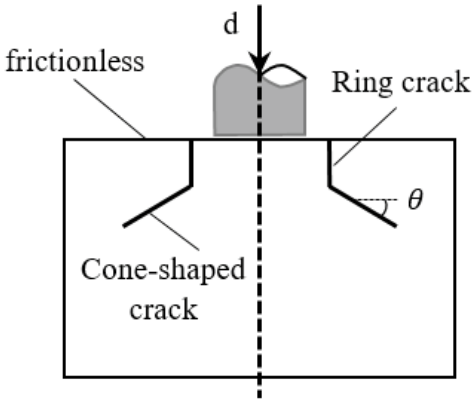

Fig. 1. Hertzian indentation fracture

2. Peridynamic theory

In this section, the peridynamic theory is briefly introduced. The peridynamic theory was first proposed by Silling (2000) as a non-local meshfree method by reformulating the equation of motion in integral form rather than the derivative of the displacements. The discretized material points can interact with each other inside a region called horizon. The interactions can be defined as peridynamic bonds. According to Silling (2000), in bond based peridynamics, the equation of motion of a material point **x** can be written as

$$\rho(\mathbf{x})\ddot{\mathbf{u}}(\mathbf{x},t)=\int_{H_{\mathbf{x}}}\mathbf{f}\left(\mathbf{u}(\mathbf{x}',t)-\mathbf{u}(\mathbf{x},t),\mathbf{x}'-\mathbf{x}\right)dV_{\mathbf{x}'}+\mathbf{b}(\mathbf{x},t) \tag{1}$$

in which ρ represents the density of the material at point $\mathbf{x}$, and $\mathbf{u}$ is the displacement at time t. $H_{\mathbf{x}}$ is the horizon centred at material point $\mathbf{x}$ while $dV_{\mathbf{x}'}$ is the infinitesimal volume of the material point $\mathbf{x}'$. $\boldsymbol{\xi}=\mathbf{x}'-\mathbf{x}$ represents the bond between $\mathbf{x}$ and $\mathbf{x}'$ indicating the relative position in the original configuration. $\mathbf{b}$ is the external force acting at the material point $\mathbf{x}$ called body force. $\mathbf{f}$ is the pairwise force function per unit volume squared which depends on the stretch of the bond and material properties.

Bond based peridynamics has a limitation that the Poisson's ratio of the material can only be 1/4 for the three-dimensional models and 1/3 for the two-dimensional models as mentioned by Madenci and Oterkus (2014). Thus, it is necessary to introduce the ordinary state based peridynamic theory for more general implementation. As derived by Silling et al. (2007), the governing equation can be rewritten as

$$\rho(\mathbf{x})\ddot{\mathbf{u}}(\mathbf{x},t)=\int_{H_{\mathbf{x}}}\left\{\underline{\mathbf{T}}[\mathbf{x},t]\langle\mathbf{x}'-\mathbf{x}\rangle-\underline{\mathbf{T}}[\mathbf{x}',t]\langle\mathbf{x}-\mathbf{x}'\rangle\right\}dV_{\mathbf{x}'}+\mathbf{b}(\mathbf{x},t) \tag{2}$$

where $\underline{\mathbf{T}}[\mathbf{x},t]\langle\mathbf{x}'-\mathbf{x}\rangle-\underline{\mathbf{T}}[\mathbf{x}',t]\langle\mathbf{x}-\mathbf{x}'\rangle$ indicates the force per unit volume squared that particle $\mathbf{x}'$ and particle $\mathbf{x}$ are exerting on each other. Here, $\underline{\mathbf{T}}$, is the force vector state at time t. It can be regarded as an output mapping from the original bond vector $\boldsymbol{\xi}=\mathbf{x}'-\mathbf{x}$. As shown in Figure 2, the direction of force vector state is parallel to the deformed bond vector $\mathbf{y}'-\mathbf{y}$ in the current configuration. Therefore, the force vector state can be expressed as

$$\underline{\mathbf{T}}\langle\mathbf{x}'-\mathbf{x}\rangle=\underline{t}\langle\mathbf{x}'-\mathbf{x}\rangle\frac{\mathbf{y}'-\mathbf{y}}{|\mathbf{y}'-\mathbf{y}|} \tag{3}$$

in which $\underline{t}$ is the magnitude of $\underline{\mathbf{T}}$ called scalar force vector state.

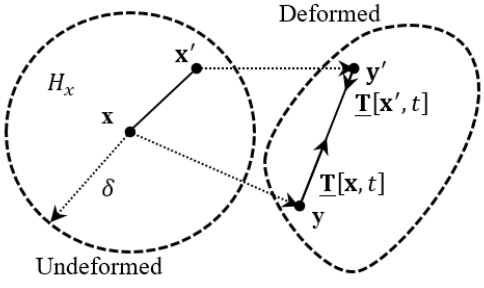

Fig. 2. Peridynamic forces in ordinary state-based peridynamics

3. Axisymmetric Peridynamic model

In the Hertzian indentation problem, since the geometry model, the external loading, and the boundary conditions are all symmetric about the central axis of the cylinder, it can be regarded as an axisymmetric problem. Thus, two-dimensional model of the cylindrical section can be considered instead of a three-dimensional cylinder, which is less time-consuming for numerical computations. To obtain the equation of motion based on the axisymmetric

peridynamic model introduced by Zhang and Qiao (2018), the expression of PD strain energy density formula needs to be proposed first. Then, by equalizing the PD energy density with the corresponding energy from classical continuum mechanics, the related parameters in the PD energy density equation can be obtained. By calculating the derivative of the PD strain energy density, we can finally get the peridynamic force vector state.

To solve the axisymmetric problem, the cylindrical coordinate is utilized in this study. In classical continuum mechanics, for the isotropic material under linear elastic deformation, the strain energy density can be expressed as

$$W_{ccm} = \frac{\lambda}{2}\Theta^2 + \mu\varepsilon_{ij}\varepsilon_{ij} \tag{4}$$

in which λ and μ are the Lame constants of the material. ε_{ij} is the strain tensor, which can be defined as

$$\varepsilon_r = \frac{\partial u_r}{\partial r}, \varepsilon_z = \frac{\partial u_z}{\partial z}, \ \varepsilon_\varphi = \frac{u_r}{r}, \ \varepsilon_{zr} = \frac{1}{2}\left(\frac{\partial u_r}{\partial z} + \frac{\partial u_z}{\partial r}\right) \tag{5}$$

where u_r and u_z are the displacement components in radial and axial directions, respectively. Θ represents the volume dilatation which can be defined as

$$\Theta = \varepsilon_r + \varepsilon_z + \varepsilon_\varphi = \frac{dS}{S} + \frac{u_r}{r} \tag{6}$$

Here, dS / S, is regarded as surface dilatation. Substituting Eqs. (5) and (6) into Eq. (4), the strain energy density in classical theory can be rewritten as

$$W_{ccm} = \frac{\lambda}{2}\left(\frac{dS}{S} + \frac{u_r}{r}\right)^2 + \mu\left(\frac{u_r}{r}\right)^2 + \mu\sum_{i,j=1,2}\varepsilon_{ij}\varepsilon_{ij} \tag{7}$$

where the indices 1,2 represent r and z, respectively.

In order to propose a suitable formula for the PD strain energy density, a new variable Θ^* is introduced as

$$\Theta^* = \frac{2\underline{\omega}\underline{x}\cdot\underline{e}}{q} \tag{8}$$

in which $\underline{\omega}$ is the influence function, having a value between 0 and 1, and only depending on the distance between the material points. $\underline{x}$ is the position scalar state indicating the original length of the bond, $\underline{e}$ represents the extension scalar state defined as $\underline{e} = \varepsilon\underline{x}$ and $\underline{q}$ is the weighted volume expressed as $q = \underline{\omega}\underline{x}\cdot\underline{x}$ (Silling et. al., 2007). The dot product is the integral of the product of two vectors as explained in Silling et. al. (2007).

To simplify the study, we assume the model is under isotropic deformation. Thus, the surface dilatation will be

$dS/S = 2\varepsilon$. Θ^* is calculated as the same value as the surface dilatation. In this way, it can be regarded as the equivalence of the surface dilatation.

By making an analogy to the equation of the classical energy density, the PD strain energy density expression is proposed as

$$W_{PD} = \frac{\lambda'}{2}\left(\Theta^* + \frac{u_r}{r}\right)^2 + \frac{\beta}{2}\left(\underline{\omega}\underline{e}\right)\cdot\underline{e} + \frac{\gamma}{2}\left(\frac{u_r}{r}\right)^2 + \alpha\,\Theta^*\left(\frac{u_r}{r}\right) \tag{9}$$

where $\alpha, \beta, \gamma, \lambda'$ are the parameters that need to be determined. The elongation $\underline{e}$ can be written as

$$\underline{e} = \frac{1}{|\xi|}\sum_{i,j=1,2}\varepsilon_{ij}\xi_i\xi_j \tag{10}$$

The representative volume element in this model is like a ring. As shown in Fig. 3, assuming the length of the bond equal to l, the infinitesimal volume dV of material point $\mathbf{x}'$ can be expressed as

$$dV_{\xi} = 2\pi\left(r + l\cos\phi\right)l\,dl\,d\phi \tag{11}$$

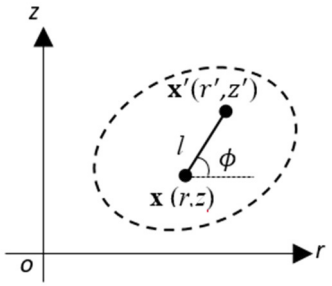

Fig. 3. A single bond in the axisymmetric model

Utilising Eqs. (10), (11) and by defining $\xi_1 = l\cos\phi$, $\xi_2 = l\sin\phi$, and δ as the horizon size, the second term of the PD energy equation given in Eq. (9) can be obtained as

$$\frac{\beta}{2}\left(\underline{\omega}\underline{e}\right)\cdot\underline{e} = \frac{\beta}{2}\int_0^{\delta}\int_0^{2\pi}\frac{\underline{\omega}\langle l\rangle}{l^2}\left[\begin{array}{l}\left(\varepsilon_{11}\right)^2\left(\xi_1\right)^4 + \left(\varepsilon_{22}\right)^2\left(\xi_2\right)^4 + 4\left(\varepsilon_{12}\right)^2\left(\xi_1\right)^2\left(\xi_2\right)^2 \\ +2\varepsilon_{11}\varepsilon_{22}\left(\xi_1\right)^2\left(\xi_2\right)^2\end{array}\right]\left(2\pi r\right)l\,dl\,d\phi \tag{12}$$

The weighted volume can be calculated as

$$q = \underline{\omega}\underline{x}\cdot\underline{x} = \int_H \underline{\omega}\langle\xi\rangle|\xi|^2\, dV_\xi = 2\pi\int_0^\delta\int_0^{2\pi}\left[\underline{\omega}\langle l\rangle l^2\left(r + l\cos\phi\right)\right] l dl d\phi = \left(2\pi\right)\left(2\pi r\right)\int_0^\delta \underline{\omega}\langle l\rangle l^3 dl \tag{13}$$

which only depends on *r*.

By considering Eq. (13), the factors associated with ε_{ij} in Eq. (12) can be calculated as

$$\int_0^\delta\int_0^{2\pi}\left[\frac{\underline{\omega}\langle l\rangle}{l^2}\left(\xi_1\right)^4\left(2\pi r\right)\right] l dl d\phi = \left(2\pi\right)\left(2\pi r\right)\int_0^\delta \underline{\omega}\langle l\rangle l^3 dl \frac{1}{2\pi}\int_0^{2\pi}\cos 4\phi d\phi = \frac{3q}{8} \tag{14}$$

$$\int_0^\delta\int_0^{2\pi}\left[\frac{\underline{\omega}\langle l\rangle}{l^2}\left(\xi_2\right)^4\left(2\pi r\right)\right] l dl d\phi = \left(2\pi\right)\left(2\pi r\right)\int_0^\delta \underline{\omega}\langle l\rangle l^3 dl \frac{1}{2\pi}\int_0^{2\pi}\sin 4\phi d\phi = \frac{3q}{8} \tag{15}$$

$$\int_0^\delta\int_0^{2\pi}\left[\frac{\underline{\omega}\langle l\rangle}{l^2}\left(\xi_1\right)^2\left(\xi_2\right)^2\left(2\pi r\right)\right] l dl d\phi = \left(2\pi\right)\left(2\pi r\right)\int_0^\delta \underline{\omega}\langle l\rangle l^3 dl \frac{1}{2\pi}\int_0^{2\pi}\sin 2\phi\cos 2\phi d\phi = \frac{q}{8} \tag{16}$$

Substituting Eqs. (14)-(16) in Eq. (12), the second term of the PD strain energy density expression can be rewritten as

$$\frac{\beta}{2}\left(\underline{\omega}\underline{e}\right)\cdot\underline{e} = \frac{\beta}{2}\left(\frac{q}{8}\left(\Theta^*\right)^2 + \frac{2q}{8}\sum_{i,j=1,2}\varepsilon_{ij}\varepsilon_{ij}\right) \tag{17}$$

Thus, the PD strain energy density expression can be rewritten as

$$W_{PD} = \left(\frac{\lambda'}{2} + \frac{\beta q}{16}\right)\left(\Theta^*\right)^2 + \left(\lambda' + \alpha\right)\Theta^*\left(\frac{u_r}{r}\right) + \left(\frac{\lambda'}{2} + \frac{\gamma}{2}\right)\left(\frac{u_r}{r}\right)^2 + \frac{\beta q}{8}\sum_{i,j=1,2}\varepsilon_{ij}\varepsilon_{ij} \tag{18}$$

Equating the PD strain energy density with the strain energy density from classical continuum mechanics, the undetermined parameters can be calculated as

$$\lambda' = \lambda - \mu\ ,\ \beta = \frac{8\mu}{q},\quad \gamma = 3\mu\ ,\ \alpha = \mu \tag{19}$$

After obtaining the PD strain energy density expression, we can calculate the scalar force state vector from the derivative of the peridynamic strain energy density W_{PD}. However, W_{PD} here is not only related to bond elongation, but also depends on the radial displacement u_r. Therefore, the increment of the PD energy is divided into two parts. One part is influenced by the bond elongation, $\left(\nabla_e W_{PD}\right)\cdot\Delta e$. The Frechet derivative of PD strain energy density,

$\nabla_e W_{PD}$, is a scalar force state. The second part arises from the increment of the radial displacement, $\left(\nabla_{u_r} W_{PD}\right)\cdot \Delta u_r$. The ordinary derivative of PD strain energy density, $\nabla_{u_r} W_{PD}$, is regarded as a body force b_r, the direction of which is always consistent with the positive *r*-axis. The scalar force state $\underline{t}$ and the body force b_r can be written, respectively, as

$$\underline{t} = \left[\lambda' \Theta^* + \left(\lambda' + \alpha\right)\frac{u_r}{r}\right]\frac{2\underline{\omega}\underline{x}}{q} + \beta \underline{\omega}\underline{e} \tag{20}$$

$$b_r = -\frac{1}{r}\left[\left(\lambda' + \alpha\right)\Theta^* + \left(\lambda' + \gamma\right)\frac{u_r}{r}\right] \tag{21}$$

4. Peridynamic contact model of axisymmetric problem

The interaction between the indenter and the cylinder needs to be considered during the contact process. When two particles are approaching very close to each other, a new type of force will be generated to prevent different material points from sharing the same position. This repelling force is calculated as a short-range force according to Madenci and Oterkus (2014) which is one of the most widely used method to depict the contact model in the peridynamic framework. Thus, as shown in Fig. 4, if the distance between two material points that belong to different bodies is less than the critical distance δ_c, a contact model is introduced. In this study, the critical distance is defined as the radius of the contact area to justify whether there is contact pairwise force between two material points in the current configuration. In Fig. 4, S represents the interface of two bodies. Since frictionless contact is assumed in the Hertzian indentation case, the friction contact force can be neglected in this study. The normal contact force state $\underline{\mathbf{T}}_n$ is proposed as an external force to represent the contact model. Therefore, by taking the contact model into consideration, the peridynamic equation of motion can be formulated as

$$\rho(\mathbf{x})\ddot{\mathbf{u}}(\mathbf{x},t) = \int_{H_\mathbf{x}} \left\{\underline{\mathbf{T}}[\mathbf{x},t]\langle\boldsymbol{\xi}\rangle - \underline{\mathbf{T}}[\mathbf{x}',t]\langle-\boldsymbol{\xi}\rangle\right\} dV_{\mathbf{x}'} + \mathbf{b}(\mathbf{x},t) + \int_{H_c} \left\{\underline{\mathbf{T}}_n[\mathbf{x},t]\langle\boldsymbol{\xi}\rangle - \underline{\mathbf{T}}_n[\mathbf{x}',t]\langle-\boldsymbol{\xi}\rangle\right\} dV_{\mathbf{x}'} \tag{22}$$

in which the normal contact force state is perpendicular to the contact interface, i.e.

$$\underline{\mathbf{T}}_n\langle\boldsymbol{\xi}\rangle = -\underline{t}_n\langle\boldsymbol{\xi}\rangle \operatorname{sgn}\left(\mathbf{Y}\langle\boldsymbol{\xi}\rangle\cdot\mathbf{e}_z\right)\mathbf{e}_z \tag{23}$$

where $\underline{t}_n$ is the scalar of the contact force state and $\mathbf{e}_z$ represents the unit vector along the z-axis direction.

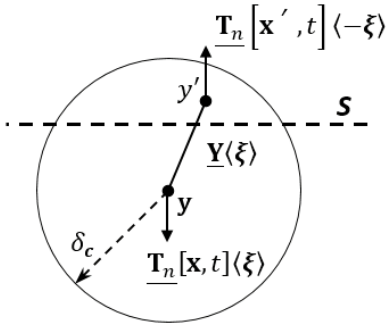

Fig. 4. Peridynamic contact model

According to the contact model used in the two-dimensional axisymmetric pull-out numerical model by Zhang and Qiao (2019), the relationship between the normal contact pressure p_c acting on the contact surface and the normal contact force state t_n can be defined as

$$t_n\langle\boldsymbol{\xi}\rangle=\begin{cases}\dfrac{3p_c}{8\pi\delta^3 r_y} & \text{if } \left|\mathbf{y}'-\mathbf{y}\right|<\delta_c \\ 0 & \text{otherwise}\end{cases} \tag{24}$$

in which r_y is radial coordinate of the material point $\mathbf{x}$ in the current configuration. Assuming there is a virtual bond between the two material points in contact, the normal contact pressure p_c can be calculated based on the stretch of the virtual bond and can be expressed as

$$p_c=E_c\left(\frac{\left|\underline{x}\cdot\mathbf{e}_y\right|-\left|\underline{y}\cdot\mathbf{e}_y\right|}{\left|\underline{x}\cdot\mathbf{e}_y\right|}\right) \tag{25}$$

where E_c is the contact stiffness and can be written as

$$\frac{1}{E_c}=\frac{1}{E_1}+\frac{1}{E_2} \tag{26}$$

5. Numerical results

In this section, numerical cases of the Hertzian indentation are simulated based on the axisymmetric peridynamic model and the numerical results will be compared with the results obtained from FEM to testify the accuracy of the axisymmetric peridynamic model. After the validation case, the crack propagation inside the cylinder will be analysed.

5.1. The axisymmetric indentation problem without fracture

The aim of this case is to verify the accuracy of the application of the axisymmetric peridynamic model for the Hertzian indentation problem. The small indenter has a radius of $r_{ind} = 5.0\times10^{-4}$ m while the radius of the cylinder is set as $r_{cyl} = 5.0\times10^{-3}$ m , i.e. 10 times larger than that of the indenter. Therefore, the effect of the edge can be neglected. The cylinder has a height of $H = 6.0\times10^{-3}$ m . The geometry can be simplified as a two-dimensional model. For the cylinder, it is uniformly discretized into 200 and 240 material points distributed along the radial and axial directions, respectively. Whereas 20 particles are located along the boundary of the indenter. The bottom of the cylinder is vertically fixed with additional three fictitious layers of material points. The vertical displacement of fictitious layers is defined as zero to constrain the bottom surface of the cylinder. The displacement of $d = 1.0\times10^{-5}$ m is applied at the top boundary of the indenter as shown in Fig. 5. Thus, there will be contact between the indenter and the cylinder with the radius of the small indenter. To implement the loading condition to the numerical model, three fictitious layers of the material points is added at the top boundary of the indenter. The material utilized in this case is the borosilicate glass with the elastic modulus of $E = 80\,\text{GPa}$, Poisson's ratio of $\nu = 0.22$, and energy release rate of $G_c = 9\,\text{J/m}^2$ (Mouginot and Maugis, 1985). Since it is a static problem, the adaptive dynamic relaxation method is implemented to ensure the convergence of the quasi-static solution. The radius of the horizon is defined as $\delta = 7.5375\times10^{-5}$ m , which is 3.015 times of the spacing between the particles. In addition, in this study we set the critical contact radius as $r_{cont} = 7.5375\times10^{-5}$ m which is the same as the horizon size.

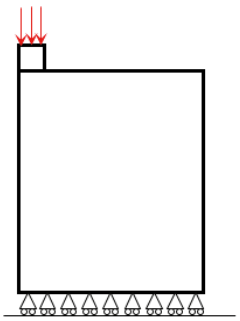

Fig. 5. Axisymmetric indentation problem

The comparison of the displacements along the radial and axial directions between the peridynamic results and the results obtained from FEM for the Hertzian indentation are shown in Fig. 6.

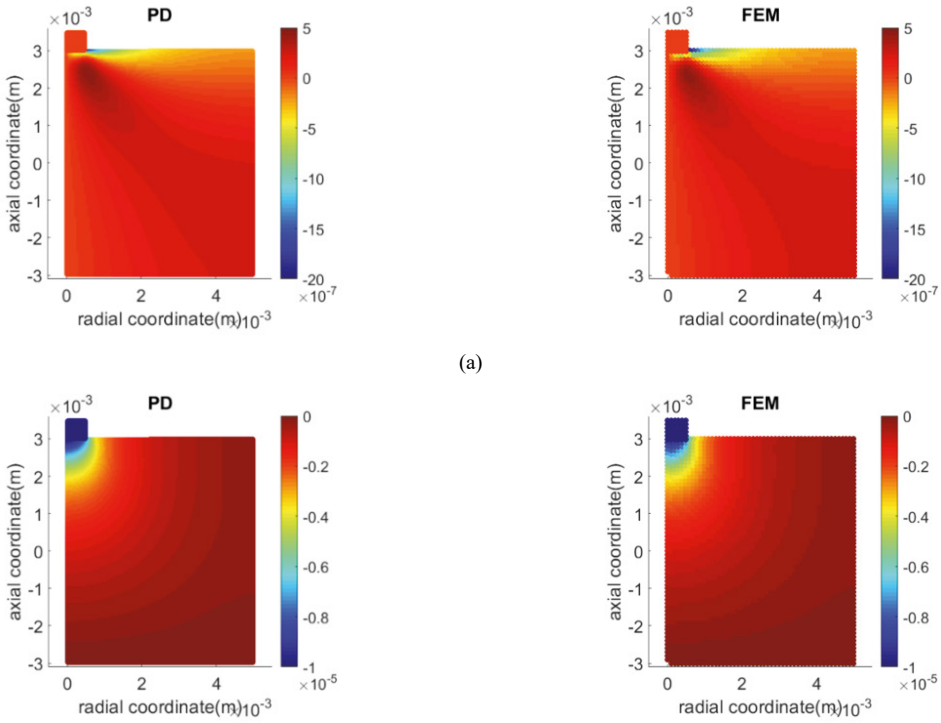

Fig. 6. The comparison of (a) radial, (b) axial displacements for the axisymmetric indentation problem.

It can be clearly seen from this figure that the displacements obtained from the axisymmetric peridynamic model agree well with the FEM result. Only some error occurs near the boundary due to incomplete horizon. Therefore, the accuracy of the axisymmetric peridynamic model is verified and the numerical model can be used for the Hertzian indentation analysis.

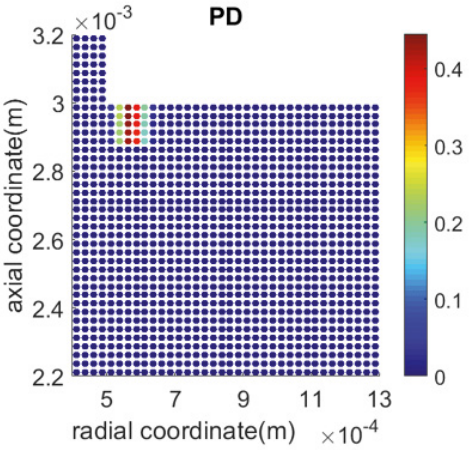

Fig. 7. The initial damage of the Hertzian indentation model

5.2. The fracture of the Hertzian indentation

A pre-existing crack near the maximum stress point located at $r_0 = 5.75\times10^{-4}$ m between two particles is inserted to investigate its propagation. The radial coordinate of the pre-existing crack is defined as $r_{crack} = 5.8\times10^{-4}$ m .The material parameters utilized in this case is same as the former case under same loading condition. The initial length of the crack is set as $a_0 = 1.25\times10^{-4}$ m which is 5 times of the distance between the particles as shown in Fig. 7. The bonds between the material points that cross the initial crack were broken to represent the failure. In order to model the bond rupture, the failure criterion is introduced. In this study, the energy criterion is considered. When the bond energy exceeds the critical energy, the bond between the material points is broken. As mentioned by Zhang and Piao (2018), the critical energy can be calculated as,

$$w_c = \frac{3G_c}{8\pi\delta^3}\left(\frac{1}{r_{\mathbf{x}}}+\frac{1}{r_{\mathbf{x}'}}\right) \tag{27}$$

In peridynamics, the energy for a single bond can be written as

$$w = \int_0^{\eta}\left(\underline{\mathbf{T}}\left[\mathbf{x},t\right]\left\langle\mathbf{x}'-\mathbf{x}\right\rangle - \underline{\mathbf{T}}\left[\mathbf{x}',t\right]\left\langle\mathbf{x}-\mathbf{x}'\right\rangle\right)\cdot d\eta \tag{28}$$

The propagation of the pre-existing crack is shown in Fig. 8. The figure at the right side indicates the detail of the crack. Initially, the ring crack vertically grows for a small distance. Then, with the increase in load, a cone crack is generated and propagates at an angle of approximately 45 degrees.

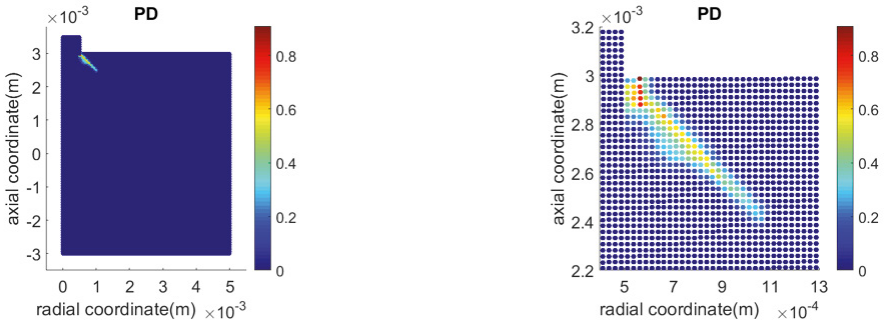

Fig. 8. The deformation and the crack propagation during the indentation

By changing the Poisson's ratio of the material and maintaining the other parameters as constant, we investigated the influence of the Poisson's ratio on the crack propagation. The results can be seen in Fig. 9. It is obvious that by increasing the value of the Poisson's ratio, the length of the propagated crack becomes shorter. The angle of cone crack maintains as 45 degrees.

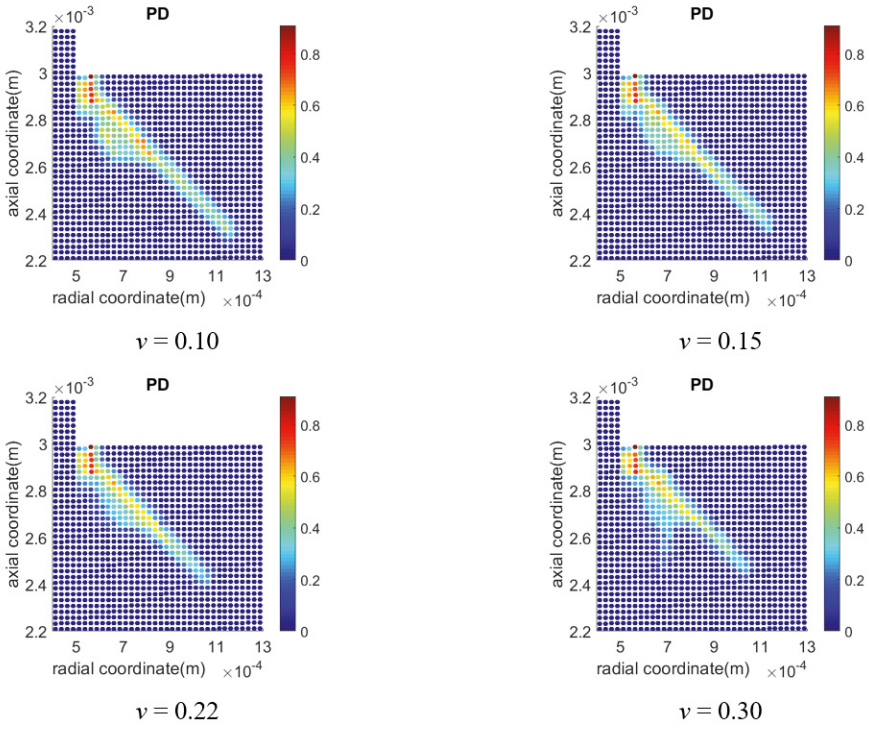

Fig. 9. The damage of the cylinder with different Poisson's ratio values

6. Conclusion

In this paper, the two-dimensional axisymmetric peridynamic model is briefly described. By equalizing the strain energy density between the peridynamics and classical continuum mechanics, the strain energy equation for axisymmetric peridynamics can be obtained. Then, the force state vector is calculated from the derivative of the strain energy. By introducing the contact model in the framework of peridynamics, the Hertzian indentation can be simulated. The validation case without fracture verifies the accuracy of the axisymmetric peridynamic model. With the energy failure criterion, the propagation of a pre-existing crack inside the brittle solid is simulated. The crack initially grew with a small distance perpendicular to the free surface of the brittle solid. Then, with the increase in load, a cone-shaped crack occurred and steadily propagated at a certain angle, approximately 45 degrees in this case. By increasing the value of the Poisson's ratio, the length of the propagated crack becomes shorter. However, the angle of cone crack maintains as 45 degrees.

Acknowledgements

The authors gratefully acknowledges the financial support from China Scholarship Council (No. 201806680018) and University of Strathclyde.

References

Basoglu, M.F., Zerin, Z., Kefal, A., Oterkus, E., 2019. A computational model of peridynamic theory for deflecting behavior of crack propagation with micro-cracks. Computational Materials Science 162, 33–46.

De Meo, D., Oterkus, E., 2017. Finite element implementation of a peridynamic pitting corrosion damage model. Ocean Engineering 135, 76–83.

Diyaroglu, C., Oterkus, S., Oterkus, E., Madenci, E., 2017a. Peridynamic modeling of diffusion by using finite-element analysis. IEEE Transactions on Components, Packaging and Manufacturing Technology 7(11), 1823–1831.

Diyaroglu, C., Oterkus, S., Oterkus, E., Madenci, E., Han, S., Hwang, Y., 2017b. Peridynamic wetness approach for moisture concentration analysis in electronic packages. Microelectronics Reliability 70, 103–111.

Diyaroglu, C., Oterkus, E., Oterkus, S., 2019. An Euler–Bernoulli beam formulation in an ordinary state-based peridynamic framework. Mathematics and Mechanics of Solids 24(2), 361–376.
Frank, F.C., Lawn, B., 1967. On the theory of Hertzian fracture. Proceedings of the Royal Society of London. Series A. Mathematical and Physical Sciences 299(1458), 291–306.
Imachi, M., Tanaka, S., Bui, T.Q., Oterkus, S., Oterkus, E., 2019. A computational approach based on ordinary state-based peridynamics with new transition bond for dynamic fracture analysis. Engineering Fracture Mechanics 206, 359–374.
Kocer, C., Collins, R.E., 1998. Angle of Hertzian cone cracks. Journal of the American Ceramic Society 81(7), 1736–1742.
Madenci, E., Oterkus, E., 2014. Peridynamic Theory and Its Applications. Springer, New York, NY.
Mouginot, R., Maugis, D., 1985. Fracture indentation beneath flat and spherical punches. Journal of Materials Science 20(12), 4354–4376.
Oliver, W.C., Pharr, G.M., 1992. An improved technique for determining hardness and elastic modulus using load and displacement sensing indentation experiments. Journal of Materials Research 7(6), 1564–1583.
Oterkus, E., Barut, A., Madenci, E., 2010a. Damage growth prediction from loaded composite fastener holes by using peridynamic theory. In 51st AIAA/ASME/ASCE/AHS/ASC Structures, Structural Dynamics, and Materials Conference 18th AIAA/ASME/AHS Adaptive Structures Conference, Orlando, Florida, USA, p. 3026.
Oterkus, E., Guven, I. and Madenci, E., 2010b. Fatigue failure model with peridynamic theory. In 12th IEEE Intersociety Conference on Thermal and Thermomechanical Phenomena in Electronic Systems, Las Vegas, Nevada, USA, p. 1-6.
Oterkus, E., Madenci, E., 2012a. Peridynamics for failure prediction in composites. In 53rd AIAA/ASME/ASCE/AHS/ASC Structures, Structural Dynamics and Materials Conference 20th AIAA/ASME/AHS Adaptive Structures Conference, Honolulu, Hawaii, USA, p. 1692.
Oterkus, E., Madenci, E., 2012b. Peridynamic theory for damage initiation and growth in composite laminate. Key Engineering Materials 488, 355–358.
Oterkus, E., Guven, I., Madenci, E., 2012. Impact damage assessment by using peridynamic theory. Open Engineering 2(4), 523–531.
Oterkus, S., Madenci, E., Oterkus, E., Hwang, Y., Bae, J., Han, S., 2014, May. Hygro-thermo-mechanical analysis and failure prediction in electronic packages by using peridynamics. In 2014 IEEE 64th Electronic Components and Technology Conference (ECTC), Orlando, Florida, USA, p. 973-982.
Selvadurai, A.P.S., 2000. Fracture evolution during indentation of a brittle elastic solid. Mechanics of Cohesive-frictional Materials: An International Journal on Experiments, Modelling and Computation of Materials and Structures 5(4), 325–339.
Silling, S.A., 2000. Reformulation of elasticity theory for discontinuities and long-range forces. Journal of the Mechanics and Physics of Solids 48(1), 175–209.
Silling, S.A., Epton, M., Weckner, O., Xu, J., Askari, E., 2007. Peridynamic states and constitutive modeling. Journal of Elasticity 88(2), 151–184.
Strobl, M., Seelig, T., 2019. Analysis of Hertzian indentation fracture using a phase field approach. PAMM 19(1), p.e201900257.
Tumbajoy-Spinel, D.Y., Feulvarch, É., Bergheau, J.M., Kermouche, G., 2013. 2D axisymmetric X-FEM modeling of the Hertzian cone crack system. Comptes Rendus Mécanique 341(9-10), 715–725.
Vazic, B., Wang, H., Diyaroglu, C., Oterkus, S., Oterkus, E., 2017. Dynamic propagation of a macrocrack interacting with parallel small cracks. AIMS Materials Science 4(1), pp.118–136.
Wang, H., Oterkus, E., Oterkus, S., 2018. Predicting fracture evolution during lithiation process using peridynamics. Engineering Fracture Mechanics 192, 176–191.
Warren, R., 1978. Measurement of the fracture properties of brittle solids by Hertzian indentation. Acta Metallurgica 26(11), 1759–1769.
Warren, P.D., 1995. Determining the fracture toughness of brittle materials by Hertzian indentation. Journal of the European Ceramic Society 15(3), 201–207.
Yang, Z., Oterkus, E., Nguyen, C.T., Oterkus, S., 2019. Implementation of peridynamic beam and plate formulations in finite element framework. Continuum Mechanics and Thermodynamics 31(1), 301–315.
Zhang, Y., Qiao, P., 2018. An axisymmetric ordinary state-based peridynamic model for linear elastic solids. Computer Methods in Applied Mechanics and Engineering 341, pp.517–550.
Zhang, Y., Qiao, P., 2019. Peridynamic simulation of two-dimensional axisymmetric pull-out tests. International Journal of Solids and Structures 168, 41–57.
Zhu, N., De Meo, D., Oterkus, E., 2016. Modelling of granular fracture in polycrystalline materials using ordinary state-based peridynamics. Materials 9(12), p.977.